

# Wasserstein Evolution : Evolutionary Optimization as Phase Transition

Kaichen Ouyang<sup>\*1</sup>

<sup>1</sup>University of Science and Technology of China, Hefei, China

## Abstract

This paper introduces a novel framework linking evolutionary computation to statistical physics by formulating optimization as a statistical phase transition. We propose Wasserstein Evolution (WE), an algorithm based on the Wasserstein gradient flow of a free energy functional, translating the physical competition between exploitative potential gradient forces and explorative entropic forces into an adaptive search mechanism. Theoretical analysis confirms WE's convergence to the Boltzmann distribution, ensuring a principled performance-diversity balance. Experiments compare WE against five established algorithms, including GA, DE, CMA-ES, JADE, and SaDE, on benchmark and physical potential functions. Results demonstrate that WE consistently achieves the lowest free energy and maintains the highest entropy, excelling in both solution quality and diversity preservation. Additional invariance tests using transformed Schwefel 2.22 functions verify that WE possesses translation, scale, and rotation invariance, proving its robustness and intrinsic alignment with the problem's geometry rather than its coordinate representation. Thus, this work delivers not only an effective and robust optimizer but also a new theoretical paradigm for understanding population-based search through statistical physics, viewing convergence as a disorder-to-order phase transition and opening new avenues for designing intelligent optimization methods.

**Keywords:** Wasserstein Evolution, Phase Transition, Free Energy Minimization, Evolutionary Optimization, Statistical Physics

## 1 Introduction

In real-world complex adaptive systems, simple local rules can spontaneously drive the system from macroscopic disorder to emergent order, achieving a collective functionality where

---

<sup>\*</sup>Correspondence: oykc@mail.ustc.edu.cn

the whole exceeds the sum of its parts. In nature, the process of biological evolution, facilitated by genetic crossover, mutation, and natural selection, shifts the genotypic distribution from regions of low fitness to those of higher fitness, a phenomenon well-modeled by evolutionary computation[1]. In physical systems, non-equilibrium thermodynamic processes, such as glass transitions, are driven from disorder toward order through free energy minimization, with statistical physics providing the theoretical formalization of these mechanisms[2]. In recent years, artificial intelligence models, particularly neural networks, demonstrate how simple connectivity rules among neurons, together with backpropagation, enable the learning of underlying data distributions for accurate prediction[3].

From an optimization perspective, evolutionary computation minimizes given objective functions by introducing the concept of fitness. Statistical physics models, in turn, drive free energy minimization spontaneously through the interplay of potential fields and entropy. Neural networks, meanwhile, fit given data by optimizing loss functions. Many studies have explored the relationship between learning and evolution, which computationally corresponds to the connection between evolutionary computation and neural networks[4]. On one hand, evolutionary algorithms serve as black-box optimizers that naturally optimize hyperparameters and architectures of neural networks—a field known as neuroevolution[5]. Research has also revealed profound links between neuroevolution and gradient-based optimization[6]. On the other hand, deep learning models, particularly neural networks, can act as surrogate models to accelerate the update process in evolutionary algorithms[7], guide the design and selection of evolutionary operators[8], or even inspire entirely new algorithms[9]. Beyond these connections, significant research has investigated the deep ties between statistical physics and neural networks. Early neural models—such as Hopfield networks[10] and Boltzmann machines—were directly inspired by statistical physics models[11]. Moreover, in recent years, theories grounded in statistical physics concepts have been developed to explain the generalization and convergence behaviors of deep learning, for instance, linking neural scaling laws to phase transition theory[12] and interpreting grokking phenomena through statistical-physical frameworks[13].

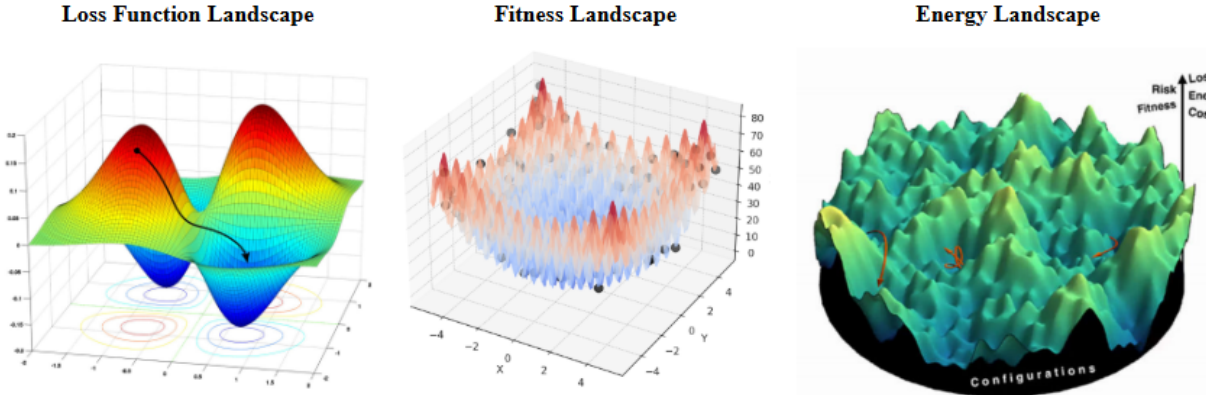


Fig. 1: Loss Function Landscape, Fitness Landscape, and Energy Landscape in Learning, Evolution, and Physical Systems

However, although extensive research has elucidated the deep connections between learning and evolution as well as between learning and physics, comparatively little attention has been paid to the relationship between evolutionary computation and statistical physics. The convergence process in evolutionary algorithms inherently involves a dynamic shift between exploration and exploitation[14]. In the initial phase, the algorithm broadly explores the solution space to identify promising regions; later, it intensively exploits these areas to refine the solution. This transition mirrors the competition observed in free energy minimization in physical systems between the potential gradient force and the entropic force[15]. The potential gradient guides the system toward lower energy states, while the entropic force drives it toward disorder, corresponding to entropy increase. Formally, the exploitation phase in evolutionary algorithms appears analogous to the role of the potential gradient force, whereas exploration resembles the entropic force. Moreover, the transition from exploration to exploitation during convergence seems to parallel the shifting dominance between these two forces as the system cools. Furthermore, the evolution of the population from initial disorder toward ordered, high-fitness regions resembles a disorder-to-order transition, akin to phase transitions such as a liquid solidifying into a solid[16]. This series of correspondences raises a fundamental question: are the parallels between evolutionary computation and statistical phase transitions merely superficial, or do they reflect a deeper mathematical duality?

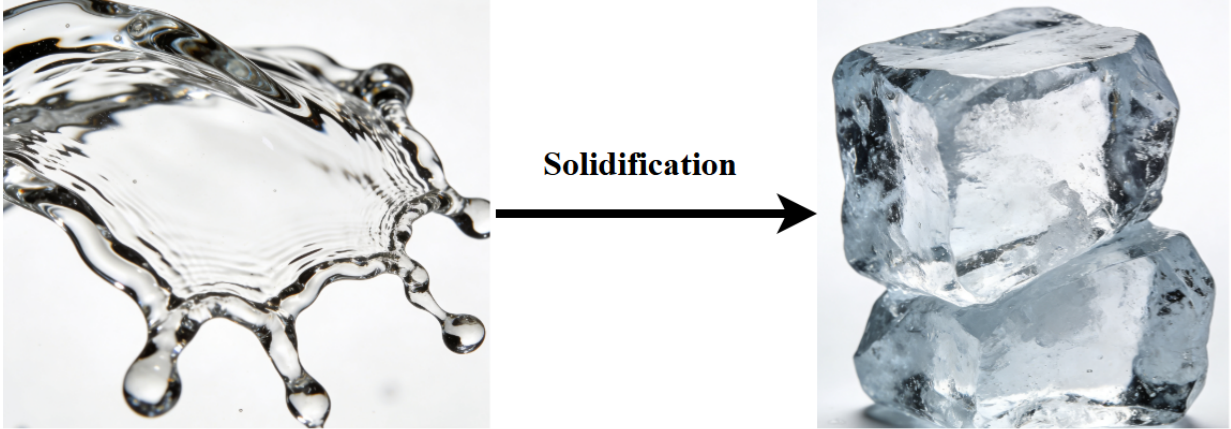


Fig. 2: The convergence of evolutionary optimization is like liquid solidification.

Inspired by this question, this study proposes Wasserstein Evolution (WE), a novel optimization framework that bridges evolutionary computation and statistical physics through the principles of Wasserstein gradient flow and free energy minimization. Experimental results demonstrate that, compared to classical evolutionary methods such as Genetic Algorithm (GA)[17], Differential Evolution (DE)[18], Covariance Matrix Adaptation Evolution Strategy (CMA-ES)[19], Adaptive Differential Evolution with Optional External Archive (JADE)[20] and Self-adaptive Differential Evolution (SaDE)[21], WE achieves excellent convergence performance on a suite of benchmark functions including Rastrigin, Beale, Himmelblau, Six-Hump Camel Back, and Holder Table, as well as on physical potential functions such as the 2D Periodic, Double-Well, Tokamak, Multipole, and Optical Lattice po-

tentials. Notably, WE achieves the lowest free energy while maintaining the highest entropy, enabling it to better capture multimodal solutions and avoid premature convergence. Theoretical analysis proves that WE converges to the Boltzmann distribution, a finding that aligns with our experimental observations. Furthermore, systematic tests on the Schwefel 2.22 function and its transformed variants verify that WE possesses translation, scale, and rotation invariance. The main contributions of this paper are summarized as follows:

1. We establish a formal correspondence between evolutionary optimization and statistical phase transition theory, proposing a free-energy-minimization-based optimization paradigm grounded in Wasserstein gradient flows.
2. We design the Wasserstein Evolution, which adaptively balances exploration and exploitation by translating the competition between potential gradient forces and entropic forces, central to physical systems, into an evolutionary optimization context.
3. We conduct extensive experiments on classical multimodal benchmark functions and real-world-inspired physical potential functions, systematically validating WE’s performance advantages. Specifically, WE consistently achieves the lowest free energy and highest entropy compared to established algorithms, including GA, DE, CMA-ES, JADE, and SaDE, demonstrating superior solution quality and sustained population diversity.
4. We demonstrate that WE possesses translation, scale, and rotation invariance through systematic tests on transformed variants of the Schwefel 2.22 function, confirming its robustness and that its dynamics are intrinsically tied to the geometry of the fitness landscape.
5. We provide a rigorous convergence analysis, proving that WE theoretically converges to the Boltzmann distribution—a result further corroborated by our experimental observations.
6. We provide novel interdisciplinary insights that reveal deep connections between optimization algorithms and physical systems, advancing the theoretical understanding of evolutionary convergence mechanisms and opening new pathways for applying statistical physics concepts in computational intelligence.

The central insight of this work is that the convergence of evolutionary algorithms can be understood as a statistical physical phase transition, with Wasserstein gradient flow offering a rigorous mathematical description of this process. This perspective not only deepens our understanding of optimization algorithms but also provides a new theoretical foundation for designing more efficient and robust intelligent optimization methods.

The remainder of this paper is organized as follows. **Section 2** introduces the fundamental background of evolutionary algorithms and phase transitions. **Section 3** elaborates on how evolutionary optimization corresponds to the phase transition process and presents the mathematical model of WE. **Section 4** presents and analyzes the performance comparison between WE and competing algorithms on benchmark test functions. Finally, **Section 5** concludes the paper and outlines potential directions for future research.

## 2 Background

### 2.1 Evolutionary Algorithms

Evolutionary algorithms (EAs) have developed as a family of population-based metaheuristic optimization methods inspired by biological evolution. The earliest and most classical form of EA can be traced back to the Genetic Algorithm (GA), introduced by Holland in 1992[17]. GA mimics natural selection by utilizing operators such as selection, crossover, and mutation to evolve a population of candidate solutions toward optimality. Subsequently, the EA framework has expanded to include several major variants, notably Differential Evolution (DE)[18] and Evolution Strategy (ES)[22]. Differential Evolution operates through vector-based mutation and crossover operations, typically employing strategies like DE/rand/1 or DE/best/1 to generate new trial vectors. Representative algorithms include DE/rand/1/bin and its adaptive successors such as JADE[20] and SHADE[23]. In contrast, Evolution Strategy emphasizes self-adaptive mutation and deterministic selection, often modeling mutation step sizes via covariance matrices, as exemplified by the well-known Covariance Matrix Adaptation Evolution Strategy (CMA-ES)[19].

Despite these developments—from classical Genetic Algorithms to Differential Evolution, Evolution Strategy, and modern variants—the core of EA design consistently revolves around balancing and transitioning between exploration and exploitation[14]. In the early iterations, algorithms prioritize exploration to broadly sample the search space and avoid premature convergence. As the evolution progresses, the focus gradually shifts toward exploitation to refine promising regions and converge to high-quality solutions. This adaptive trade-off between global search and local refinement remains a foundational principle in evolutionary computation.

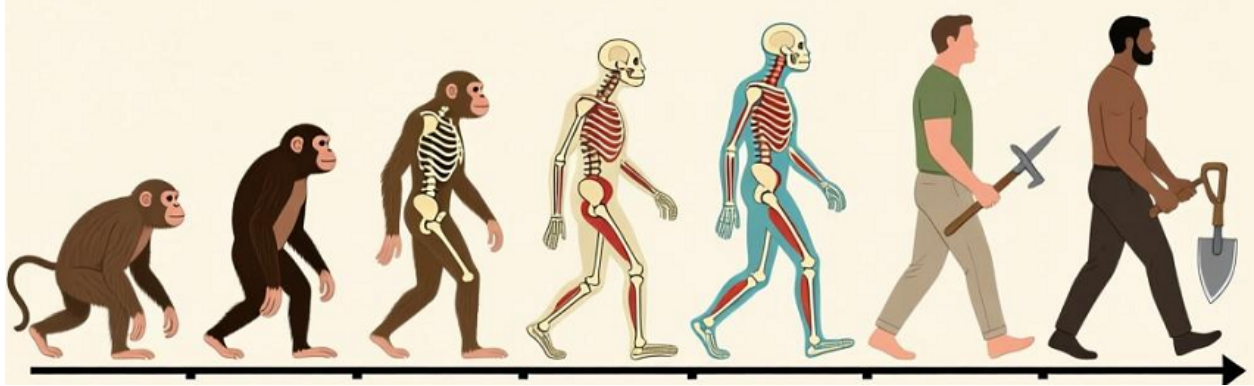


Fig. 3: The evolution of humanity

## 2.2 Phase Transition

Phase transitions in physics describe fundamental transformations between different states of matter, with common examples including liquid–solid transitions (freezing)[24], gas–liquid transitions (condensation)[25], and magnetic transitions[26]. A particularly illustrative example is the solidification process of a liquid upon cooling. During this phase transition, the system is driven by the interplay of two competing forces: the potential energy gradient, which favors the ordered, low-energy solid state, and the entropic force, which promotes the disordered, high-entropy liquid state. The potential gradient drives the system toward configurations with lower energy, while entropy resists complete ordering by maintaining thermal fluctuations and configurational diversity[27, 28].

As temperature decreases, the balance shifts in favor of the potential term, and the system undergoes a transition from a disordered liquid phase to an ordered solid phase. This progression from disorder to order bears a striking resemblance to the exploration–exploitation transition in evolutionary algorithms. In the early stages of evolution, high population entropy corresponds to broad exploration of the search space (analogous to the disordered liquid phase). Over time, selection pressure increases, entropy decreases, and the population converges toward optimal solutions (analogous to the ordered solid phase). Thus, the thermodynamics of phase transitions provides a natural physical metaphor for understanding how evolutionary algorithms dynamically shift from exploration to exploitation during optimization.

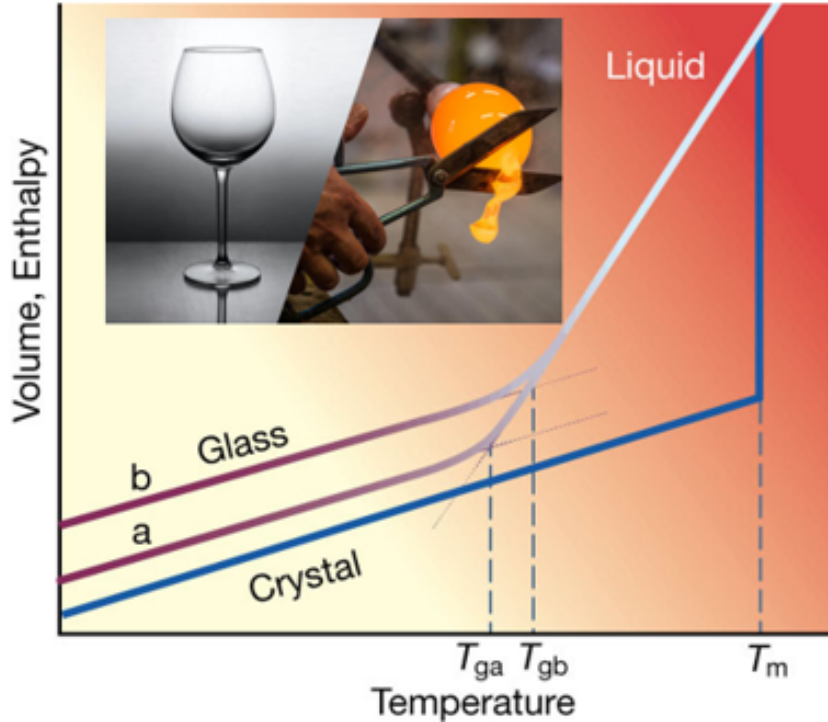


Fig. 4: Glass Transition in Liquid-Solid Phase Transition[29]

### 3 Evolutionary Optimization as Phase Transition

#### 3.1 Physical Background

The Wasserstein Evolution (WE) is grounded in three interconnected mathematical frameworks from statistical physics: Wasserstein gradient flow, the Fokker-Planck equation, and free energy minimization. Together, these provide a unified physical interpretation of evolutionary optimization as a phase transition process.

The Wasserstein gradient flow generalizes gradient descent to the space of probability measures. For a functional  $\mathcal{F}[\rho]$  defined on probability distributions, its gradient flow follows:

$$\frac{\partial \rho_t}{\partial t} = \nabla \cdot \left( \rho_t \nabla \frac{\delta \mathcal{F}[\rho_t]}{\delta \rho} \right), \quad (1)$$

where  $\frac{\delta \mathcal{F}}{\delta \rho}$  is the functional derivative and  $\rho_t(\mathbf{x})$  is the probability density at time  $t$ . This establishes steepest descent in the Wasserstein geometry of probability spaces.

The Fokker-Planck equation describes probability density evolution for stochastic systems:

$$\frac{\partial \rho_t}{\partial t} = \nabla \cdot [\rho_t \nabla f(\mathbf{x})] + D \nabla^2 \rho_t, \quad (2)$$

which governs the overdamped Langevin dynamics  $d\mathbf{x}_t = -\nabla f(\mathbf{x}_t)dt + \sqrt{2D}d\mathbf{W}_t$ . Here,  $f(\mathbf{x})$  represents the energy landscape and  $D$  is the diffusion coefficient.

Free energy minimization characterizes equilibrium thermodynamics through the functional:

$$\mathcal{F}_\beta[\rho] = \mathbb{E}_\rho[f(\mathbf{x})] - \frac{1}{\beta}S[\rho], \quad (3)$$

where  $S[\rho]$  is Shannon entropy and  $\beta$  is inverse temperature. The minimizing distribution is the Gibbs equilibrium  $\rho_{\text{eq}}(\mathbf{x}) = Z^{-1}e^{-\beta f(\mathbf{x})}$ .

These frameworks unify when we consider the specific free energy  $\mathcal{F}_\beta[\rho]$ . Its Wasserstein gradient flow becomes:

$$\frac{\partial \rho_t}{\partial t} = \nabla \cdot [\rho_t \nabla f(\mathbf{x})] + \frac{1}{\beta} \nabla^2 \rho_t, \quad (4)$$

which is exactly the Fokker-Planck equation with  $D = 1/\beta$ . This reveals that free energy minimization, implemented via Wasserstein gradient flow, produces the stochastic dynamics of the Fokker-Planck system. Consequently, WE can be viewed as a thermodynamic process where a population evolves to minimize free energy, undergoing a controlled phase transition from high-temperature, high-entropy exploration to low-temperature, low-entropy exploitation through inverse temperature annealing.

### 3.2 Wasserstein Evolution

Building upon the theoretical foundations of Wasserstein gradient flow and free energy minimization, we propose the Wasserstein Evolution (WE), which explicitly formulates evolutionary optimization as a phase transition process. WE directly implements the mean-field equation derived from the Wasserstein gradient flow of the free energy functional:

---

**Algorithm 1** Wasserstein Evolution (WE)

---

```

1: Initialize population  $\{\mathbf{x}_i^{(0)}\}_{i=1}^N \sim \text{Uniform}(\Omega)$ 
2: for  $k = 0, 1, \dots, K - 1$  do
3:   Compute current inverse temperature:  $\beta_k$ 
4:   Estimate density:  $\hat{\rho}_k(\mathbf{x})$ 
5:   for  $i = 1$  to  $N$  do
6:     Compute fitness gradient:  $\nabla f(\mathbf{x}_i^{(k)})$ 
7:     Compute entropic force:  $\nabla \log \hat{\rho}_k(\mathbf{x}_i^{(k)})$ 
8:     Update position:  $\mathbf{x}_i^{(k+1)} = \mathbf{x}_i^{(k)} + \eta_k \left[ -\nabla f(\mathbf{x}_i^{(k)}) - \frac{1}{\beta_k} \nabla \log \hat{\rho}_k(\mathbf{x}_i^{(k)}) \right]$ 
9:   end for
10:  Return free energy  $\mathcal{F}$ , entropy  $S$ , best fitness  $f^*$ , best solution  $\mathbf{x}^*$ 
11: end for
12: return Best solution  $\mathbf{x}^*$  and corresponding fitness  $f(\mathbf{x}^*)$ 

```

---

The WE comprises three key components: **(1) Density Estimation** ( $\hat{\rho}_k$ ), which ap-

proximates the population distribution at each iteration; **(2) Temperature Scheduling** ( $\beta_k$ ), which controls the exploration-exploitation trade-off through an annealing scheme; and **(3) Force Composition** ( $-\nabla f - \frac{1}{\beta_k} \nabla \log \hat{\rho}_k$ ), which combines the gradient of the objective function with the entropic term to drive the population dynamics.

WE provides a principled approach to evolutionary optimization that explicitly models the exploration-exploitation trade-off as a physical phase transition. By directly implementing the Wasserstein gradient flow of free energy, WE maintains theoretical coherence while achieving practical optimization performance, as demonstrated in our experimental results.

### 3.3 Convergence Analysis of the Wasserstein Evolution

We provide a comprehensive convergence analysis of the Wasserstein Evolution (WE). The algorithm operates on a search space  $\mathcal{X} \subseteq \mathbb{R}^d$  with objective function  $f : \mathcal{X} \rightarrow \mathbb{R}$ . We consider the minimization problem where we aim to find  $\min_{x \in \mathcal{X}} f(x)$ . At each iteration  $t$ , the algorithm maintains  $N$  particles  $X_t^{(1)}, X_t^{(2)}, \dots, X_t^{(N)}$  that evolve according to deterministic dynamics.

The core update equation for each particle is given by:

$$\frac{dX^{(i)}}{dt} = -\nabla f(X^{(i)}) - \frac{1}{\beta_t} \nabla \log \rho_t(X^{(i)}), \quad (5)$$

where  $\rho_t(x)$  represents the probability density of the particle distribution at time  $t$ , and  $\beta_t > 0$  is the inverse temperature parameter that varies with time. The first term  $-\nabla f(X^{(i)})$  drives particles toward regions of lower function values (for minimization problems), while the second term  $-\frac{1}{\beta_t} \nabla \log \rho_t(X^{(i)})$  acts as a repulsive entropic force that prevents particle concentration and maintains diversity.

Rather than analyzing individual particle trajectories, we consider the evolution of the entire probability distribution  $\rho_t(x)$ . The empirical distribution formed by the particles approximates this continuous density. The relationship between particle motion and distribution evolution is governed by the continuity equation, which states that the change in probability density equals the negative divergence of the probability flux. Substituting the velocity field from equation (5) yields the partial differential equation:

$$\frac{\partial \rho_t(x)}{\partial t} = -\nabla \cdot \left[ \rho_t(x) \left( -\nabla f(x) - \frac{1}{\beta_t} \nabla \log \rho_t(x) \right) \right]. \quad (6)$$

This equation describes how the probability distribution evolves over time in response to the combined forces of potential gradient and entropic repulsion.

To analyze convergence, we introduce the free energy functional defined as:

$$\mathcal{F}_{\beta_t}[\rho] = \mathbb{E}_{x \sim \rho}[f(x)] - \frac{1}{\beta_t} S[\rho], \quad (7)$$

where  $S[\rho] = -\int \rho(x) \log \rho(x) dx$  is the (negative) Shannon entropy. The first term  $\mathbb{E}_{x \sim \rho}[f(x)] = \int f(x) \rho(x) dx$  represents the average objective function value, while the second term  $-\frac{1}{\beta_t} S[\rho]$  represents the entropic contribution. Note that since  $S[\rho]$  is negative,  $-S[\rho]/\beta_t$  is positive, which encourages entropy maximization. The free energy functional serves as a Lyapunov function for the dynamics.

We now compute the time derivative of the free energy along the solution trajectory of equation (6). First, we compute the functional derivative:

$$\frac{\delta \mathcal{F}_{\beta_t}[\rho]}{\delta \rho(x)} = f(x) + \frac{1}{\beta_t} (\log \rho(x) + 1). \quad (8)$$

The time derivative is then:

$$\frac{d}{dt} \mathcal{F}_{\beta_t}[\rho_t] = \int_{\mathcal{X}} \frac{\delta \mathcal{F}_{\beta_t}[\rho_t]}{\delta \rho(x)} \frac{\partial \rho_t(x)}{\partial t} dx. \quad (9)$$

Substituting equation (6) gives:

$$\frac{d}{dt} \mathcal{F}_{\beta_t}[\rho_t] = \int_{\mathcal{X}} \left[ f(x) + \frac{1}{\beta_t} (\log \rho_t(x) + 1) \right] \quad (10)$$

$$\times \left( -\nabla \cdot \left[ \rho_t(x) \left( -\nabla f(x) - \frac{1}{\beta_t} \nabla \log \rho_t(x) \right) \right] \right) dx. \quad (11)$$

Applying integration by parts with the assumption that boundary terms vanish (which holds for compact domains or rapidly decaying distributions), we obtain:

$$\frac{d}{dt} \mathcal{F}_{\beta_t}[\rho_t] = \int_{\mathcal{X}} \nabla \left[ f(x) + \frac{1}{\beta_t} (\log \rho_t(x) + 1) \right] \quad (12)$$

$$\cdot \left[ \rho_t(x) \left( -\nabla f(x) - \frac{1}{\beta_t} \nabla \log \rho_t(x) \right) \right] dx. \quad (13)$$

Evaluating the gradient inside the integral yields:

$$\frac{d}{dt} \mathcal{F}_{\beta_t}[\rho_t] = \int_{\mathcal{X}} \rho_t(x) \left( \nabla f(x) + \frac{1}{\beta_t} \nabla \log \rho_t(x) \right) \quad (14)$$

$$\cdot \left( -\nabla f(x) - \frac{1}{\beta_t} \nabla \log \rho_t(x) \right) dx. \quad (15)$$

This simplifies to:

$$\frac{d}{dt} \mathcal{F}_{\beta_t}[\rho_t] = - \int_{\mathcal{X}} \rho_t(x) \left\| \nabla f(x) + \frac{1}{\beta_t} \nabla \log \rho_t(x) \right\|^2 dx \leq 0. \quad (16)$$

Equation (16) shows that the free energy is non-increasing along the trajectory, establishing  $\mathcal{F}_{\beta_t}[\rho_t]$  as a valid Lyapunov function. The dissipation rate is zero if and only if  $\nabla f(x) + \frac{1}{\beta_t} \nabla \log \rho_t(x) = 0$  for all  $x$  in the support of  $\rho_t$ .

At equilibrium, when  $\frac{\partial \rho_t}{\partial t} = 0$ , equation (6) implies that the probability flux vanishes, leading to:

$$\rho_t(x) \left( -\nabla f(x) - \frac{1}{\beta_t} \nabla \log \rho_t(x) \right) = 0. \quad (17)$$

Assuming  $\rho_t(x) > 0$  almost everywhere, this reduces to:

$$-\nabla f(x) - \frac{1}{\beta_t} \nabla \log \rho_t(x) = 0, \quad (18)$$

which is equivalent to  $\nabla f(x) + \frac{1}{\beta_t} \nabla \log \rho_t(x) = 0$ , consistent with the condition for zero dissipation in equation (16).

Rearranging equation (18) gives  $\nabla \log \rho_t(x) = -\beta_t \nabla f(x)$ . Integrating both sides with respect to  $x$  yields:

$$\log \rho_t(x) = -\beta_t f(x) + C, \quad (19)$$

where  $C$  is an integration constant. Exponentiating produces:

$$\rho_t(x) = e^C \cdot e^{-\beta_t f(x)}. \quad (20)$$

Normalizing to obtain a valid probability density function gives the equilibrium distribution:

$$\rho_{\text{eq}}(x) = \frac{1}{Z_{\beta_t}} e^{-\beta_t f(x)}, \quad (21)$$

where  $Z_{\beta_t} = \int_{\mathcal{X}} e^{-\beta_t f(x)} dx$  is the partition function ensuring  $\int \rho_{\text{eq}}(x) dx = 1$ .

This equilibrium distribution is precisely the Boltzmann distribution with energy function  $f(x)$  (for minimization). The parameter  $\beta_t$  controls the concentration of the distribution: when  $\beta_t$  is small, the distribution is diffuse and exploratory; when  $\beta_t$  is large, the distribution concentrates on regions where  $f(x)$  is minimized.

To establish convergence to this equilibrium, we examine the behavior of the free energy functional at the equilibrium distribution. Substituting equation (21) into equation (7) gives:

$$\mathcal{F}_{\beta_t}[\rho_{\text{eq}}] = \frac{1}{Z_{\beta_t}} \int f(x) e^{-\beta_t f(x)} dx - \frac{1}{\beta_t} S[\rho_{\text{eq}}]. \quad (22)$$

Using the properties of the Boltzmann distribution, we can show that for the specific form  $\rho_{\text{eq}}(x) = e^{-\beta_t f(x)} / Z_{\beta_t}$ , the entropy is given by:

$$S[\rho_{\text{eq}}] = \log Z_{\beta_t} + \beta_t \mathbb{E}_{\rho_{\text{eq}}}[f(x)]. \quad (23)$$

Substituting equation (23) into the free energy expression yields:

$$\mathcal{F}_{\beta_t}[\rho_{\text{eq}}] = -\frac{1}{\beta_t} \log Z_{\beta_t}. \quad (24)$$

This represents the minimum possible value of the free energy functional for fixed  $\beta_t$ . Indeed, for any distribution  $\rho$ , we have:

$$\mathcal{F}_{\beta_t}[\rho] - \mathcal{F}_{\beta_t}[\rho_{\text{eq}}] = \frac{1}{\beta_t} D_{\text{KL}}(\rho \parallel \rho_{\text{eq}}) \geq 0, \quad (25)$$

where  $D_{\text{KL}}$  is the Kullback-Leibler divergence, which is non-negative.

The convergence argument proceeds as follows. Equation (16) shows that the free energy decreases monotonically along the trajectory. Combined with the lower bound in equation (25), this ensures convergence to the equilibrium distribution. Moreover, as  $\beta_t$  increases over time (a process called annealing), the equilibrium distribution becomes increasingly concentrated on the global minimum of  $f(x)$ .

In the limit  $\beta_t \rightarrow \infty$ , the Boltzmann distribution converges weakly to a Dirac delta distribution centered on the global minimum:

$$\lim_{\beta_t \rightarrow \infty} \rho_{\text{eq}}(x) = \delta(x - x^*), \quad (26)$$

where  $x^* = \arg \min_{x \in \mathcal{X}} f(x)$ , assuming the minimum is unique. For multiple global minima, the distribution converges to a mixture of Dirac deltas at each global minimum.

The mathematical rigor of this convergence is supported by the fact that the dynamics constitute a gradient flow in the space of probability measures equipped with the Wasserstein metric. The free energy functional is geodesically convex under appropriate conditions on  $f(x)$ , ensuring exponential convergence to equilibrium. The discrete-time implementation with finite particle count introduces approximation errors, but these can be controlled through the choice of kernel bandwidth in density estimation and through the learning rate in the discretization of equation (5).

The WE thus provides a principled approach to global optimization that combines gradient-based local search with entropy-driven exploration. The theoretical guarantee of convergence to the Boltzmann distribution ensures that, with appropriate annealing of  $\beta_t$ , the algorithm will eventually concentrate its search effort on the globally optimal regions

of the search space, while maintaining diversity through the entropy term to escape local optima during the initial phases of optimization.

## 4 Experiments

### 4.1 Experimental Setup

We conducted comprehensive experiments to evaluate Wasserstein Evolution (WE) against five established evolutionary algorithms: Genetic Algorithm (GA)[17], Differential Evolution (DE)[18], Covariance Matrix Adaptation Evolution Strategy (CMA-ES)[19], Adaptive Differential Evolution with Optional External Archive (JADE)[20], and Self-adaptive Differential Evolution (SaDE)[21].

The test suite comprises ten functions, categorized into two types: five classical mathematical benchmark functions and five physical potential energy functions. The benchmark functions were selected for their diverse characteristics including multimodality, symmetry, and deceptive landscapes. The physical potential functions model complex real-world systems such as crystal adsorption, molecular conformation transitions, magnetic confinement plasmas, ion traps, and optical lattices. These two categories provide complementary testbeds for assessing algorithmic performance on both abstract mathematical landscapes and physically meaningful energy surfaces. Details of all test functions are provided in Table 1. All algorithms were configured with a population size of  $N = 30$  and executed for  $K = 500$  iterations, with each experiment repeated 30 times for statistical reliability.

Performance is assessed using two complementary metrics computed from the final population. The first is the **Average Free Energy**  $\mathcal{F}$ , calculated as:

$$\mathcal{F} = \mathbb{E}_\rho[U] - \frac{1}{\beta}S \quad (27)$$

where  $U(\mathbf{x}_i)$  is the objective function value (potential energy) and  $\beta$  is the final inverse temperature. This composite metric directly reflects the algorithm's ability to balance energy minimization with entropy preservation.

The second is the **Average Differential Entropy**  $S$ , which quantifies the population's configurational diversity. For a final population  $\{\mathbf{x}_i\}_{i=1}^N$ , the entropy is estimated via multi-variate Gaussian Kernel Density Estimation (KDE):

$$S = -\frac{1}{N} \sum_{i=1}^N \log \hat{\rho}(\mathbf{x}_i), \quad (28)$$

where  $\hat{\rho}$  is the KDE estimate. Higher entropy values indicate more diverse, multi-modal

population distributions, reflecting stronger exploration capacity. Together, these metrics provide a comprehensive evaluation framework grounded in statistical physics principles.

Table 1: Benchmark and Physical Potential Functions Used in the Experiments

Category	Name & Formula	Domain	Features / Physical Interpretation
Benchmark	<b>Rastrigin:</b> $f(\mathbf{x}) = 10n + \sum_{i=1}^n [x_i^2 - 10 \cos(2\pi x_i)]$	$[-5.12, 5.12]^2$	Highly multimodal, separable. Global optimum: $f(\mathbf{0}) = 0$ .
	<b>Beale:</b> $f(x, y) = (1.5 - x + xy)^2 + (2.25 - x + xy^2)^2 + (2.625 - x + xy^3)^2$	$[-4.5, 4.5]^2$	Non-convex, unimodal with a narrow valley. Global optimum: $f(3, 0.5) = 0$ .
	<b>Himmelblau:</b> $f(x, y) = (x^2 + y - 11)^2 + (x + y^2 - 7)^2$	$[-6, 6]^2$	Symmetric with four equal-valued global minima ( $f^* = 0$ ).
	<b>Six-Hump Camel:</b> $f(x, y) = x \in [-3, 3], y \in [-2, 2] \left( 4 - 2.1x^2 + \frac{x^4}{3} \right) x^2 + xy + (-4 + 4y^2)y^2$	$[-10, 10]^2$	Two global minima ( $f \approx -1.0316$ ) and four local minima.
	<b>Holder Table:</b> $f(x, y) = -\left  \sin(x) \cos(y) \exp \left( \left  1 - \frac{\sqrt{x^2 + y^2}}{\pi} \right  \right) \right $	$[-10, 10]^2$	Highly multimodal. Four global minima ( $f \approx -19.2085$ ).
Physical Potential	<b>2D Periodic:</b> $V = -V_0 [\cos(\frac{2\pi x}{a}) + \cos(\frac{2\pi y}{a}) + \lambda_c \cos(\frac{2\pi x}{a}) \cos(\frac{2\pi y}{a})], V_0 = 2.0, a = 1.0, \lambda_c = 0.5$	$[-2, 2]^2$	Periodic potential for crystal adsorption. Symmetric lattice wells.
	<b>Double-Well:</b> $V = (x^2 - 1)^2 + \frac{1}{2}ky^2 + A_g \exp[-B(x^2 + y^2)], k = 2.0, A_g = 3.0, B = 3.0$	$[-2, 2]^2$	Molecular conformation transitions. Two metastable states separated by a Gaussian barrier.
	<b>Tokamak:</b> $V = \alpha(r - r_0)^2 + \beta(r - r_0)^4 + \epsilon(r - r_0) \cos(m\theta) + \delta \cos(n\theta), r_0 = 2.0, \alpha = 0.5, \beta = 0.05, \epsilon = 0.8, \delta = 0.6, m = 3, n = 2$	$[-4, 4]^2$	Charged particle drift in tokamak fields. Magnetic islands create multiple metastable states.
	<b>Multipole:</b> $V = \sum_{i=1}^4 \frac{s_i q}{4\pi\epsilon_0 \sqrt{(x-x_i)^2 + (y-y_i)^2 + \delta^2}}, q = 1.0, \epsilon_0 = 1.0, \delta = 0.3$	$[-3, 3]^2$	Quadrupole ion trap potential. Alternating charges create saddle points and trapping regions.
	<b>Optical Lattice:</b> $V = V_0 [\sin^2(kx) + \sin^2(ky)] \exp\left[-\frac{x^2 + y^2}{2\sigma^2}\right], V_0 = 3.0, k = 2.0, \sigma = 3.0$	$[-4, 4]^2$	Optical lattice for cold atoms. Periodic modulation with Gaussian envelope creates multiple traps.

## 4.2 Experiments on Test Functions

The performance of all six algorithms across the ten test functions is summarized in Table 2. Each cell reports the average Free Energy  $\mathcal{F}$  and the corresponding average differential Entropy  $S$  over 30 independent runs.

Table 2: Average Free Energy  $\mathcal{F}$  and Entropy  $S$  of WE and Competitors

Function (Metric)	WE	GA	DE	CMA-ES	JADE	SaDE
Rastrigin ( $\mathcal{F}$ )	<b>-0.0039</b>	0.0698	0.0343	0.0342	0.0343	0.0344
Rastrigin ( $S$ )	<b>3.8783</b>	-34.3251	-34.2552	-34.2164	-34.3120	-34.3626
Beale ( $\mathcal{F}$ )	<b>0.0018</b>	0.3087	0.0343	0.0343	0.0343	0.0343
Beale ( $S$ )	<b>-1.7029</b>	-33.1249	-34.3191	-34.3006	-34.3421	-34.3226
Himmelblau ( $\mathcal{F}$ )	<b>-0.0039</b>	0.0405	0.0343	0.0090	0.0343	0.0343
Himmelblau ( $S$ )	<b>3.9380</b>	-34.3633	-34.3011	-5.9218	-34.3114	-34.2870
Six-Hump Camel ( $\mathcal{F}$ )	<b>-1.0332</b>	-0.9971	-0.9973	-1.0271	-0.9979	-0.9973
Six-Hump Camel ( $S$ )	<b>1.6167</b>	-34.3446	-34.2828	-4.5358	-33.7709	-34.3261
Holder Table ( $\mathcal{F}$ )	<b>-19.2146</b>	-19.1732	-19.0401	-19.1743	-19.1771	-19.1752
Holder Table ( $S$ )	<b>6.1341</b>	-33.7130	-32.1155	1.2729	-31.3723	-33.2832
2D Periodic ( $\mathcal{F}$ )	<b>-5.0032</b>	-4.9656	-4.9895	-4.9995	-4.9834	-4.9966
2D Periodic ( $S$ )	<b>3.1528</b>	-34.2458	-10.4928	-0.4719	-16.5898	-3.4461
Double-Well ( $\mathcal{F}$ )	<b>0.1190</b>	0.1520	0.1502	0.1207	0.1490	0.1520
Double-Well ( $S$ )	<b>-1.2880</b>	-34.3109	-32.5156	-2.9730	-31.2836	-34.3225
Tokamak ( $\mathcal{F}$ )	<b>-0.6927</b>	-0.6559	-0.6570	-0.6898	-0.6570	-0.6563
Tokamak ( $S$ )	<b>2.8447</b>	-33.9353	-32.8931	-0.0087	-32.8407	-33.4977
Multipole ( $\mathcal{F}$ )	<b>-0.2185</b>	-0.1808	-0.1820	-0.2068	-0.1815	-0.1803
Multipole ( $S$ )	<b>3.8663</b>	-33.6437	-32.5899	-7.7928	-33.0796	-34.3084
Optical Lattice ( $\mathcal{F}$ )	<b>-0.0042</b>	0.0335	0.0343	-0.0034	0.0317	0.0343
Optical Lattice ( $S$ )	<b>4.1921</b>	-33.4341	-34.3124	4.0787	-31.7351	-34.3470

The results clearly show that the proposed WE consistently achieves the lowest free energy values across all ten test functions. This aligns with the theoretical intuition that the Wasserstein gradient flow follows the steepest descent path for free energy minimization. Furthermore, WE maintains the highest entropy among all compared algorithms, which is consistent with the theoretical expectation that the optimal population distribution should converge to the Boltzmann distribution at equilibrium. The performance superiority of WE holds for both classical mathematical benchmarks and physically inspired potential functions, demonstrating its robustness and generalizability across diverse and complex landscapes.

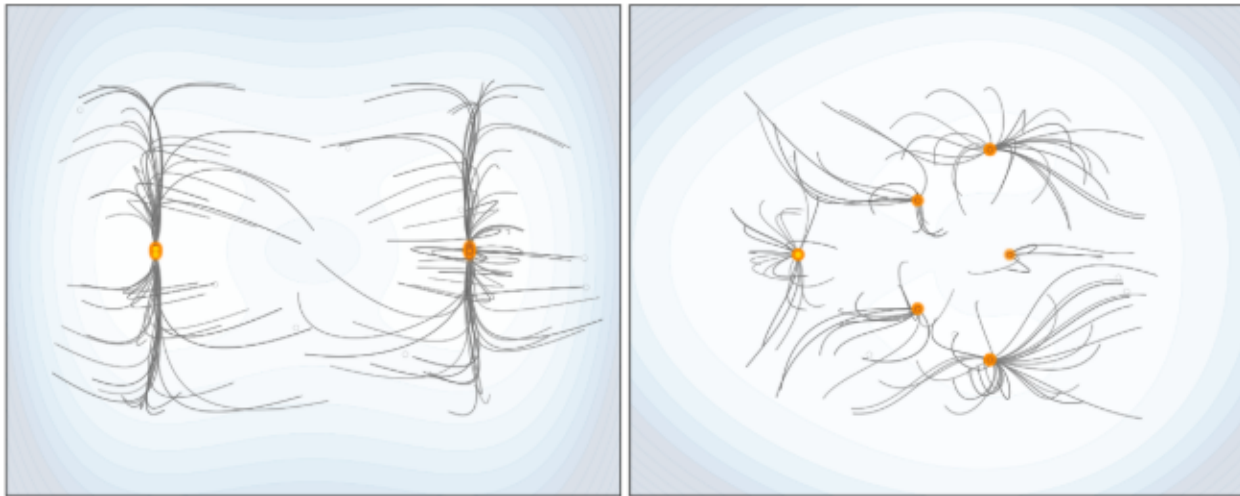


Fig. 5: Trajectories of the Population in WE

To further investigate the phase transition behavior of WE and verify its convergence to the Boltzmann distribution, we conducted additional analyses on selected complex landscapes. Taking the Himmelblau, Six-Hump Camel Back, Double-Well, and Tokamak functions as examples, we visualize both the final population distribution and the search trajectories.

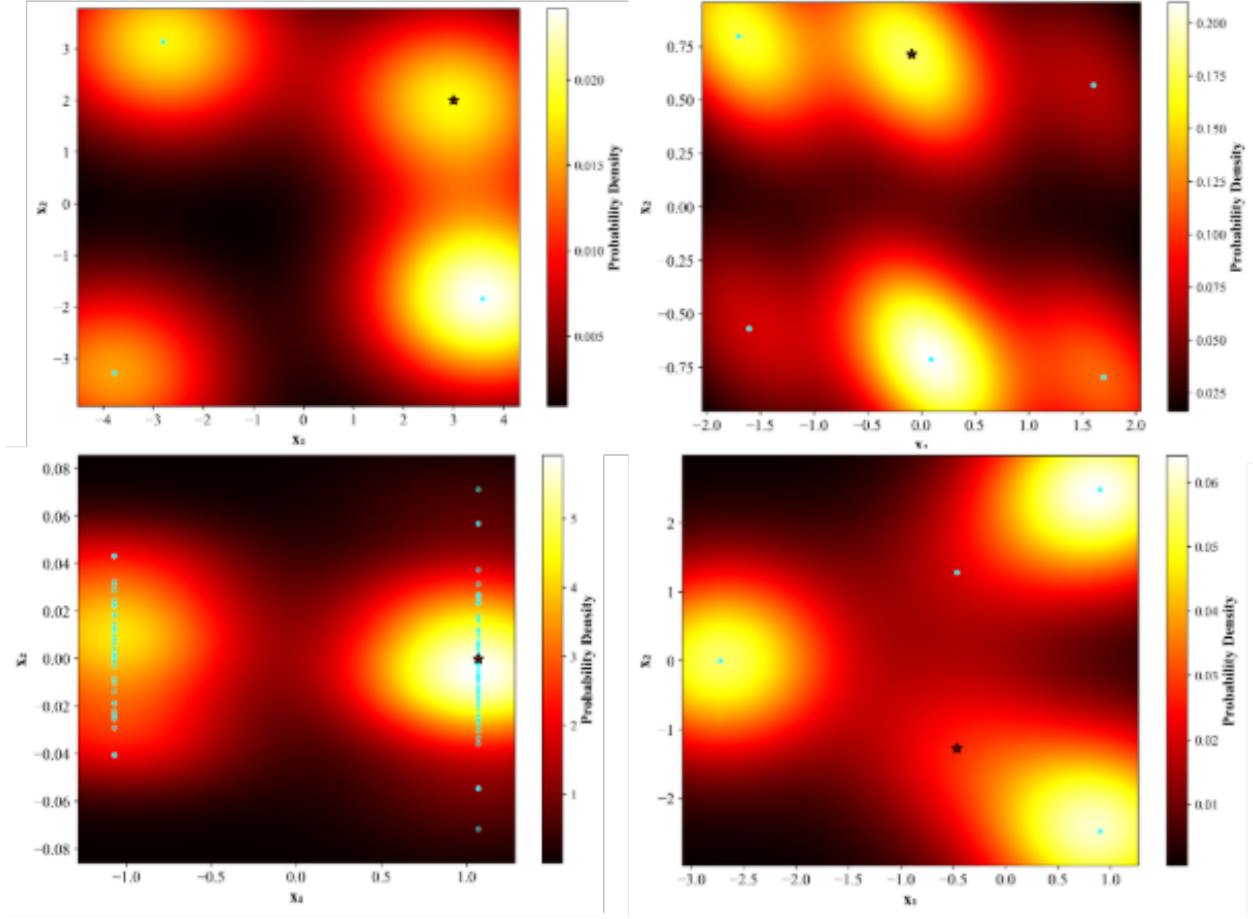


Fig. 6: Probability Density Heatmap of the Final Population in WE

Figure 6 presents probability density heatmaps of WE’s final populations. These visualizations confirm that the empirical distribution aligns with the theoretical Boltzmann distribution, as regions with lower energy exhibit higher population density. Notably, the density peaks correspond exactly to the multiple minima of each function, providing empirical evidence that WE effectively samples from the Boltzmann distribution and successfully locates multiple optima in complex landscapes. Figure 5 illustrates the convergence process by showing the search trajectories of individual particles. The trajectories reveal how particles, driven by the combined forces of potential gradient and entropy, gradually navigate from broadly distributed initial positions toward the low-energy regions. This process visually manifests the phase transition from a high-entropy, exploratory state (disorder) to a low-entropy, concentrated state (order) around the optimal solutions, consistent with the theoretical interpretation of optimization as a free-energy-minimization-driven phase transition.

### 4.3 Translation, Scale, and Rotation Invariance of WE

A robust optimization algorithm should ideally possess certain invariances to basic transformations of the search space. Specifically, translation, scale, and rotation invariance are desirable properties[30, 31]. **Translation invariance** ensures that an algorithm’s performance does not depend on the absolute location of the optimum in the search space. **Scale invariance** implies that the algorithm performs consistently regardless of the units or magnitude scaling of the decision variables. **Rotation invariance** is crucial for handling non-separable problems, as it ensures the algorithm is not biased towards the original coordinate axes. For gradient-based or geometry-aware algorithms like WE, which utilize both the gradient of the objective function ( $\nabla f$ ) and the gradient of the population density ( $\nabla \log \rho$ ), verifying these invariances is essential to confirm that its dynamics are fundamentally tied to the intrinsic geometry of the fitness landscape rather than its specific parameterization.

To systematically test these properties of WE, we employ the Schwefel 2.22 function as a base function and construct a suite of transformed variants, as detailed in Table 3. These variants include pure translation, scaling, rotation, and composite transformations that combine all three operations in different sequences. If WE exhibits the aforementioned invariances, its convergence behavior, final free energy, and entropy should remain statistically consistent across the original function and all its transformed versions, except for predictable shifts or scaling in the solution values themselves. The following experiments and analyses are designed to investigate this hypothesis.

Table 3: Schwefel 2.22 Function and Its Transformations for Invariance Testing

Category	Name & Transformation Description	Domain	Mathematical Form / Notes
Base Function	Original Schwefel 2.22	$[-100, 100]^2$	$f(\mathbf{x}) = \sum_{i=1}^n \left( \sum_{j=1}^i x_j \right)^2, n = 2.$ The global minimum is $f(\mathbf{0}) = 0$ .
Translation	Schwefel 2.22-Shift Right 20	$[-100, 100]^2$	$\mathbf{x}_{\text{trans}} = \mathbf{x} - 20$ . Minimum at $\mathbf{x}^* = (20, 20)$ .
	Schwefel 2.22-Shift Left 30	$[-100, 100]^2$	$\mathbf{x}_{\text{trans}} = \mathbf{x} + 30$ . Minimum at $\mathbf{x}^* = (-30, -30)$ .
	Schwefel 2.22-Shift (15, 15)	$[-100, 100]^2$	$x_{\text{trans},0} = x_0 - 15, x_{\text{trans},1} = x_1 - 15$ . Minimum at $\mathbf{x}^* = (15, 15)$ .
Scaling	Schwefel 2.22-Scale x2 (Enlarge)	$[-100, 100]^2$	$\mathbf{x}_{\text{trans}} = \mathbf{x} \times 0.5$ . Function landscape is enlarged by a factor of 2.
	Schwefel 2.22-Scale x0.5 (Reduce)	$[-100, 100]^2$	$\mathbf{x}_{\text{trans}} = \mathbf{x} \times 2.0$ . Function landscape is shrunk by half.
	Schwefel 2.22-Anisotropic Scale	$[-100, 100]^2$	$x_1 = x_1 \times 0.6667, x_2 = x_2 \times 1.25$ . Different scaling per axis.
Rotation	Schwefel 2.22-Rotate 45°	$[-100, 100]^2$	$\mathbf{x}_{\text{trans}} = R(45^\circ) \mathbf{x}$ , where $R$ is a 2D rotation matrix.
	Schwefel 2.22-Rotate -30°	$[-100, 100]^2$	$\mathbf{x}_{\text{trans}} = R(-30^\circ) \mathbf{x}$ .
	Schwefel 2.22-Rotate 75°	$[-100, 100]^2$	$\mathbf{x}_{\text{trans}} = R(75^\circ) \mathbf{x}$ .
Composite	Schwefel 2.22-Translate-Rotate-Scale	$[-100, 100]^2$	Sequence: Translate by $(10, -10) \rightarrow$ Rotate 60° $\rightarrow$ Scale (0.8, 1.2).
	Schwefel 2.22-Rotate-Translate-Scale	$[-100, 100]^2$	Sequence: Rotate 45° $\rightarrow$ Translate by $(15, -15) \rightarrow$ Scale (0.7, 1.5).

### Schwefel 2.22 Function Variants: Contour Plots

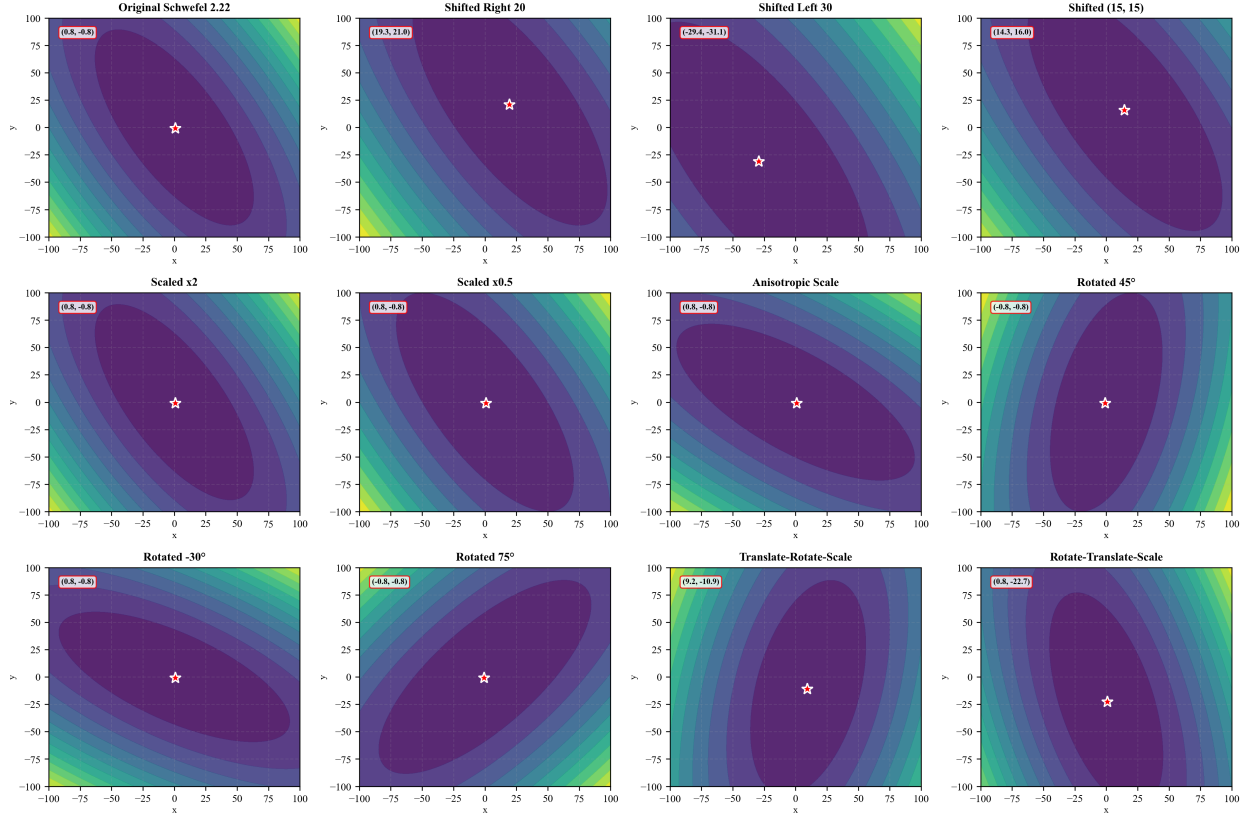


Fig. 7: Contour plots of the Schwefel 2.22 function and its transformed variants.

Table 4: Average Free Energy  $\mathcal{F}$  and Entropy  $S$  of WE and Competitors on Schwefel 2.22 Transformations

Function (Metric)	WE	GA	DE	CMA-ES	JADE	SaDE
Original ( $\mathcal{F}$ )	<b>0.0057</b>	0.4980	0.0343	0.0344	0.0344	0.0343
Original ( $S$ )	<b>-5.7499</b>	-33.7497	-34.3451	-34.3637	-34.3649	-34.3328
Shift Right 20 ( $\mathcal{F}$ )	<b>0.0057</b>	0.7317	0.0343	0.0344	0.0343	0.0343
Shift Right 20 ( $S$ )	<b>-5.7420</b>	-33.3897	-34.3341	-34.3665	-34.2949	-34.2984
Shift Left 30 ( $\mathcal{F}$ )	<b>0.0062</b>	0.6788	0.0343	0.0343	0.0343	0.0343
Shift Left 30 ( $S$ )	<b>-6.1653</b>	-33.8295	-34.3042	-34.3201	-34.3101	-34.2928
Shift (15, 15) ( $\mathcal{F}$ )	<b>0.0058</b>	0.4777	0.0343	0.0344	0.0343	0.0343
Shift (15, 15) ( $S$ )	<b>-5.7807</b>	-33.2944	-34.3173	-34.3684	-34.3241	-34.3355
Scale x2 ( $\mathcal{F}$ )	<b>0.0076</b>	0.1423	0.0343	0.0343	0.0343	0.0343
Scale x2 ( $S$ )	<b>-7.1719</b>	-33.8689	-34.2644	-34.2716	-34.3068	-34.2746
Scale x0.5 ( $\mathcal{F}$ )	<b>0.0067</b>	2.0389	0.0343	0.0343	0.0344	0.0344
Scale x0.5 ( $S$ )	<b>-6.6958</b>	-33.7282	-34.2921	-34.3427	-34.3565	-34.3706
Anisotropic Scale ( $\mathcal{F}$ )	<b>0.0056</b>	0.3047	0.0343	0.0343	0.0344	0.0343
Anisotropic Scale ( $S$ )	<b>-5.6218</b>	-33.7350	-34.3409	-34.2988	-34.3905	-34.3028
Rotate 45° ( $\mathcal{F}$ )	<b>0.0052</b>	0.2298	0.0343	0.0344	0.0343	0.0344
Rotate 45° ( $S$ )	<b>-5.1908</b>	-33.1372	-34.3493	-34.3539	-34.3287	-34.3611
Rotate -30° ( $\mathcal{F}$ )	<b>0.0057</b>	0.5717	0.0343	0.0343	0.0343	0.0343
Rotate -30° ( $S$ )	<b>-5.6895</b>	-34.3541	-34.2934	-34.2986	-34.2988	-34.2832
Rotate 75° ( $\mathcal{F}$ )	<b>0.0060</b>	0.4285	0.0344	0.0343	0.0343	0.0344
Rotate 75° ( $S$ )	<b>-5.9855</b>	-34.3367	-34.3740	-34.3358	-34.3411	-34.3876
Translate-Rotate-Scale ( $\mathcal{F}$ )	<b>0.0052</b>	0.2658	0.0343	0.0343	0.0344	0.0343
Translate-Rotate-Scale ( $S$ )	<b>-5.1885</b>	-34.3381	-34.3096	-34.3098	-34.3963	-34.3146
Rotate-Translate-Scale ( $\mathcal{F}$ )	<b>0.0053</b>	0.2223	0.0343	0.0343	0.0343	0.0343
Rotate-Translate-Scale ( $S$ )	<b>-5.3402</b>	-34.3666	-34.3172	-34.3149	-34.2942	-34.2662

The quantitative results presented in Table 4 provide compelling empirical evidence for the translation, scale, and rotation invariance of Wasserstein Evolution (WE). Across all

twelve variants of the Schwefel 2.22 function, WE consistently maintains the \*\*lowest free energy\*\* values (all within the narrow range of **0.0052–0.0076**) and the **highest entropy** values (ranging from **-5.2 to -7.2**). This remarkable stability in both performance metrics, regardless of the applied transformation, directly demonstrates WE’s invariance properties. In stark contrast, while other algorithms like DE, CMA-ES, JADE, and SaDE achieve similarly low free energy values, they do so at the cost of near-zero population diversity, with entropy values consistently around **-34.3**. This indicates a complete collapse of the population distribution, revealing that these methods achieve convergence primarily through aggressive exploitation, effectively sacrificing exploration. The Genetic Algorithm (GA) further illustrates this trade-off, exhibiting not only low diversity but also significantly worse (higher) free energy values across all transformations.

These findings strongly support the central hypothesis of this section: the dynamics of WE are fundamentally tied to the intrinsic geometry of the fitness landscape. The algorithm’s update rule—a balance between the objective function gradient ( $\nabla f$ ) and the population density gradient ( $\nabla \log \rho$ )—enables it to **adapt its search direction** relative to the distribution of individuals, rather than relying on fixed, absolute coordinates. Consequently, when the search space is translated, scaled, or rotated, the **relative relationship** between the gradient forces and the entropic repulsion within the population is preserved. This allows WE to maintain a consistent balance between exploration and exploitation, leading to statistically invariant performance outcomes. This inherent invariance is a key advantage for real-world optimization problems where the optimal coordinate system or scaling is not known *a priori*, making WE a robust and versatile optimization framework.

## 5 Conclusion

This paper establishes a novel theoretical and algorithmic framework that bridges evolutionary optimization with statistical physics through the lens of phase transition theory. We rigorously formalize the convergence dynamics of evolutionary algorithms as a free energy minimization process via Wasserstein gradient flows. Building upon this foundation, we propose Wasserstein Evolution (WE), an algorithm that explicitly models the exploration-exploitation trade-off as a competition between potential gradient forces and entropic forces, mirroring the disorder-to-order transition observed in physical systems. Theoretical analysis demonstrates that WE converges to the Boltzmann distribution, ensuring a principled balance between solution quality and diversity.

The core contributions of this work are threefold. First, we establish a formal mathematical correspondence between evolutionary optimization and statistical phase transitions, providing a unified theoretical perspective on population-based search. Second, we design WE, which implements the Wasserstein gradient flow of free energy, naturally balancing exploration and exploitation through temperature-controlled entropy dynamics. Third, ex-

tensive experiments validate WE’s superior performance against five established algorithms, including GA, DE, CMA-ES, JADE, and SaDE, on a diverse suite of benchmark and physical potential functions. The results show that WE consistently achieves the lowest free energy and maintains the highest entropy upon convergence. Furthermore, systematic invariance tests on transformed variants of the Schwefel 2.22 function confirm that WE possesses translation, scale, and rotation invariance, demonstrating its robustness and intrinsic alignment with the problem geometry rather than its specific parameterization.

Looking forward, several promising research directions emerge from this work. First, future studies should extend the comparison of WE with more advanced evolutionary algorithms, including state-of-the-art variants like L-SHADE and neuroevolution-based approaches. Second, the application scope of WE can be significantly expanded to various real-world optimization problems. Notably, WE’s ability to maintain population diversity makes it particularly suitable for neural network training, where it could help escape local minima and discover more robust solutions. Similarly, in neural architecture search (NAS), WE’s exploration capabilities could facilitate discovering diverse and efficient architectures beyond those found by gradient-based NAS methods. Additionally, engineering optimization problems with complex, multi-modal landscapes—such as structural design, parameter tuning in control systems, and portfolio optimization—represent natural domains where WE’s balanced search strategy could yield substantial benefits.

Beyond these applied directions, theoretical investigations into the critical behavior of WE, particularly the characterization of phase transition points and scaling laws in high-dimensional optimization landscapes, would deepen our understanding of the algorithm’s fundamental properties. Furthermore, exploring connections between WE and other gradient flow-based methods in machine learning, such as Stein Variational Gradient Descent (SVGD) and their extensions, could lead to new hybrid algorithms with enhanced capabilities.

In conclusion, this work has laid the groundwork for viewing evolutionary optimization through the powerful lens of statistical physics. By framing optimization as a phase transition process, we have not only developed a novel algorithm with desirable properties but also opened new avenues for interdisciplinary research that connects computational intelligence with fundamental physical principles.

## References

- [1] Xingyu Wu, Sheng-hao Wu, Jibin Wu, Liang Feng, and Kay Chen Tan. Evolutionary computation in the era of large language model: Survey and roadmap. *IEEE Transactions on Evolutionary Computation*, 2024.
- [2] Jonathan Asher Pachter, Ying-Jen Yang, and Ken A Dill. Entropy, irreversibility and

inference at the foundations of statistical physics. *Nature Reviews Physics*, 6(6):382–393, 2024.

- [3] David E Rumelhart, Geoffrey E Hinton, and Ronald J Williams. Learning representations by back-propagating errors. *nature*, 323(6088):533–536, 1986.
- [4] Jun Zhang, Zhi-hui Zhan, Ying Lin, Ni Chen, Yue-jiao Gong, Jing-hui Zhong, Henry SH Chung, Yun Li, and Yu-hui Shi. Evolutionary computation meets machine learning: A survey. *IEEE Computational Intelligence Magazine*, 6(4):68–75, 2011.
- [5] Akbar Telikani, Amirkhessam Tahmassebi, Wolfgang Banzhaf, and Amir H Gandomi. Evolutionary machine learning: A survey. *ACM Computing Surveys (CSUR)*, 54(8):1–35, 2021.
- [6] Stephen Whitelam, Viktor Selin, Sang-Won Park, and Isaac Tamblyn. Correspondence between neuroevolution and gradient descent. *Nature communications*, 12(1):6317, 2021.
- [7] Yaochu Jin. Surrogate-assisted evolutionary computation: Recent advances and future challenges. *Swarm and Evolutionary Computation*, 1(2):61–70, 2011.
- [8] Shengcai Liu, Caishun Chen, Xinghua Qu, Ke Tang, and Yew-Soon Ong. Large language models as evolutionary optimizers. In *2024 IEEE Congress on Evolutionary Computation (CEC)*, pages 1–8. IEEE, 2024.
- [9] He Yu and Jing Liu. Exploring automated algorithm design synergizing large language models and evolutionary algorithms: Survey and insights. *Evolutionary Computation*, pages 1–27, 2025.
- [10] John J Hopfield. Neural networks and physical systems with emergent collective computational abilities. *Proceedings of the national academy of sciences*, 79(8):2554–2558, 1982.
- [11] David H Ackley, Geoffrey E Hinton, and Terrence J Sejnowski. A learning algorithm for boltzmann machines. *Cognitive science*, 9(1):147–169, 1985.
- [12] Jared Kaplan, Sam McCandlish, Tom Henighan, Tom B Brown, Benjamin Chess, Rewon Child, Scott Gray, Alec Radford, Jeffrey Wu, and Dario Amodei. Scaling laws for neural language models. *arXiv preprint arXiv:2001.08361*, 2020.
- [13] Ziming Liu, Ouail Kitouni, Niklas S Nolte, Eric Michaud, Max Tegmark, and Mike Williams. Towards understanding grokking: An effective theory of representation learning. *Advances in Neural Information Processing Systems*, 35:34651–34663, 2022.
- [14] Matej Črepinšek, Shih-Hsi Liu, and Marjan Mernik. Exploration and exploitation in evolutionary algorithms: A survey. *ACM computing surveys (CSUR)*, 45(3):1–33, 2013.

- [15] David Chandler. Introduction to modern statistical. *Mechanics*. Oxford University Press, Oxford, UK, 5(449):11, 1987.
- [16] Marc Mezard and Andrea Montanari. *Information, physics, and computation*. Oxford University Press, 2009.
- [17] John H Holland. Genetic algorithms. *Scientific american*, 267(1):66–73, 1992.
- [18] Rainer Storn and Kenneth Price. Differential evolution—a simple and efficient heuristic for global optimization over continuous spaces. *Journal of global optimization*, 11(4):341–359, 1997.
- [19] Nikolaus Hansen and Andreas Ostermeier. Completely derandomized self-adaptation in evolution strategies. *Evolutionary computation*, 9(2):159–195, 2001.
- [20] Jingqiao Zhang and Arthur C Sanderson. Jade: adaptive differential evolution with optional external archive. *IEEE Transactions on evolutionary computation*, 13(5):945–958, 2009.
- [21] A Kai Qin and Ponnuthurai N Suganthan. Self-adaptive differential evolution algorithm for numerical optimization. In *2005 IEEE congress on evolutionary computation*, volume 2, pages 1785–1791. IEEE, 2005.
- [22] Hans-Georg Beyer and Hans-Paul Schwefel. Evolution strategies—a comprehensive introduction. *Natural computing*, 1(1):3–52, 2002.
- [23] Ryoji Tanabe and Alex Fukunaga. Success-history based parameter adaptation for differential evolution. In *2013 IEEE congress on evolutionary computation*, pages 71–78. IEEE, 2013.
- [24] ADJ Haymet. Theory of the equilibrium liquid-solid transition. *Annual Review of Physical Chemistry*, 38(1):89–108, 1987.
- [25] DA Beysens and Yves Garrabos. The phase transition of gases and liquids. *Physica A: Statistical Mechanics and its Applications*, 281(1-4):361–380, 2000.
- [26] Barry A Cipra. An introduction to the ising model. *The American Mathematical Monthly*, 94(10):937–959, 1987.
- [27] Rudolf Clausius. *Ueber verschiedene für die Anwendung bequeme Formen der Hauptgleichungen der mechanischen Wärmetheorie: vorgetragen in der naturforsch. Gesellschaft den 24. April 1865*. Verlag nicht ermittelbar, 1865.
- [28] Josiah Willard Gibbs. *Elementary principles in statistical mechanics: developed with especial reference to the rational foundations of thermodynamics*. C. Scribner's sons, 1902.

- [29] J Jackle. Models of the glass transition. *Reports on Progress in Physics*, 49(2):171, 1986.
- [30] Jakub Kudela. A critical problem in benchmarking and analysis of evolutionary computation methods. *Nature Machine Intelligence*, 4(12):1238–1245, 2022.
- [31] Ye Tian, Xingyi Zhang, Cheng He, Kay Chen Tan, and Yaochu Jin. Principled design of translation, scale, and rotation invariant variation operators for metaheuristics. *Chinese Journal of Electronics*, 32(1):111–129, 2023.